ARTICLE

Oxygen Electroreduction Performance of Ultrasmall Gold Nanoclusters

Ting Huang, Zhi-hu Sun, Guo-qiang Pan*

National Synchrotron Radiation Laboratory, University of Science and Technology of China, Hefei 230029, China

Ultrasmall gold nanoclusters consisting of 2−4 Au atoms were synthesized and their performance in electrocatalytic oxygen reduction reactions (ORR) was examined. These clusters were synthesized by exposing $AuPPh_3Cl$ to the aqueous ammonia medium for one week. Electrospray ionization mass spectrometry (ESI-MS), X-ray absorption fine structure (XAFS), and X-ray photoelectron spectroscopy (XPS) analyses indicate that the as-synthesized gold clusters (abbreviated as Au_x) consist of 2−4 Au atoms coordinated by the triphenylphosphine, hydroxyl, and adsorbed oxygen ligands. A glassy carbon disk electrode loaded with the Aux clusters (Au_x/GC) was characterized by the cyclic and linear-sweep voltammetry for ORR. The cyclic voltammogram *vs.* RHE shows the onset potential of 0.87 V, and the kinetic parameters of J_K at 0.47 V and the electron-transfer number per oxygen molecule were calculated to be 14.28 mA/cm^2 and 3.96 via the Koutecky-Levich equations, respectively.

Key words: Ultrasmall gold nanoclusters, Synthesis, Oxygen reduction reactions, Electro-catalyst

I. INTRODUCTION

Oxygen reduction reactions (ORR) at the cathode in fuel cells have attracted extensive attention for decades on the research of effective electrocatalysts. So far, even though considerable studies have revealed the active performances of the platinum and platinum-based alloys electrocatalysts [1−13], the high expenses and limited resources restrain their widespread applications in practice. Consequently, it is of great necessity and importance to explore other non-platinum electrocatalysts which are expected to be widely employed as commercial fuel cells in the future.

Though the non-platinum bulk metals (gold, silver, and copper) are known as inert materials, their catalytic behaviors for ORR, nevertheless, become active with the size being lessened to nanometer dimension. For the ORR, the metal nanoparticle catalytic activity is intimately dependent on the oxygen absorption ability of the surface. The nanoparticles (<2 nm) exhibit active surfaces due to the lower coordination number of the surface atoms, and their electrocatalytic performances are influenced by the nanoparticle size effect. The 3 nm gold nanoparticle electrocatalyst favors the more effective four-electron ORR than the two-electron ORR of 7 nm gold nanoparticle electrocatalyst [14], the 0.7 nm silver nanocluster electrocatalyst for ORR shows

150 mV more positive onset potential and five times higher current density *vs.* Ag/AgCl at −0.80 V than that of 3.3 nm silver nanoparticle electrocatalyst [15]; the Cu nanocluster (<1 nm) electrocatalyst exhibits 120 mV more positive onset potential and ∼2.4 times higher current density *vs.* Ag/AgCl at −0.30 V than that of 10.8 nm Cu nanoparticle electrocatalyst [16]. Recent theoretical researches have indicated that the smaller Au clusters are favorable for oxygen molecule absorption due to the narrower gap between the d-band and the Fermi level [17]. With this context, the series of Au nanoclusters (<2 nm) with 11 to 140 Au atom have been examined as electrocatalysts for ORR, and the smallest Au_{11} (0.8 nm) cluster in subnanocluster scale (<1 nm) shows much better electrocatalytic activity of 150 mV positive onset potential (−0.1 mV) and 10.5 times higher current density (17.9 mA/cm^2) *vs.* Ag/AgCl at −0.5 V than that of Au_{140} (1.7 nm) cluster in nanocluster scale (<2 nm) [18]. This suggests that the small gold clusters are exceptionally effective for electrocatalytic ORR and their electrocatalytic performance for ORR deserves further investigations.

In this work, we prepared ultrasmall gold clusters of 2−4 Au atoms (Au_x) and investigated their electrocatalytic performance for ORR. The Au_x clusters, synthesized by a facile method of exposing the $AuPPh_3Cl$ to the aqueous ammonia solution for one week at room temperature, were monitored by electrospray ionization mass spectrometry (ESI-MS), X-ray absorption fine structure (XAFS) and X-ray photoelectron spectroscopy (XPS). The results indicate that the Au_x clusters are constituted of Au_2-Au_4 clusters of triph-

---

*Author to whom correspondence should be addressed. E-mail: gqpan@ustc.edu.cn

enylphosphine, hydroxyl, and adsorbed oxygen ligands. The Au_x clusters were then loaded onto a glassy carbon (Au_x/GC) electrode, and characterized by cyclic and linear-sweep voltammetry for ORR in aqueous solution of 0.1 mol/L KOH. The cyclic voltammogram of Au_x/GC *vs.* RHE shows the onset potential of 0.87 V and the peak current density of 2.0 mA/cm^2. The linear-sweep voltammograms were analyzed by the Koutecky-Levich equations, yielding the kinetic limiting current (J_K) of 14.28 mA/cm^2 at 0.47 V and the number of 3.96 electrons transferred per O_2 molecule.

II. EXPERIMENTS

A. Chemicals

Choroauric acid ($HAuCl_4$) and triphenylphosphine (99%) were purchased from Alfa Aesar. Sodium borohydride (98%) and aqueous ammonia (25 wt%) were provided by Aldrich. The $AuPPh_3Cl$ was prepared according to the method reported in Ref.[19].

B. Synthesis of ultrasmall gold clusters

The $AuPPh_3Cl$ precursor (0.4 mmol) was suspended in 10 mL of $NH_3 \cdot H_2O$ and 10 mL of ethanol solution for one week. The resulting solvent was dried in a rotary evaporator; the precipitate was dissolved in ethanol. The undissolved solid was discarded after the centrifugation at rotation rate of 15000 r/min for 5 min; the remaining supernatant was dried again, giving the cluster product ($\sim$20% yield on Au basis).

C. ESI-MS, XAS, and XPS characterizations

The molecular composition of the Au_x clusters was detected by ESI-MS, which was achieved via a Bruker Microtof mass-spectrometer operating in positive ionization mode with the temperature of 100 °C and the nitrogen drying gas of 1 μL/min in ESI source. In addition, calibration was performed by reserpine (m/z=609) in FIA 10 pg (100:1 S/N=200 μL/min). The measurement of Au_x clusters (10 μL) mass spectrum was conducted at flow rate of 0.1 mL/min in 0.1% formic acid in acetonitrile/H_2O (1:1). The measurement Au L_3-edge X-ray absorption spectroscopy (XAS) was carried out in transmission mode at the 1W1B beamline of Beijing Synchrotron Radiation Facility (BSRF), China, with electron storage ring operated at 2.5 GeV and a maximum current of 250 mA. XPS data were collected by using a VG Thermo ESCALAB 250 spectrometer operated at 120 W with the binding energy calibrated against the C 1s line.
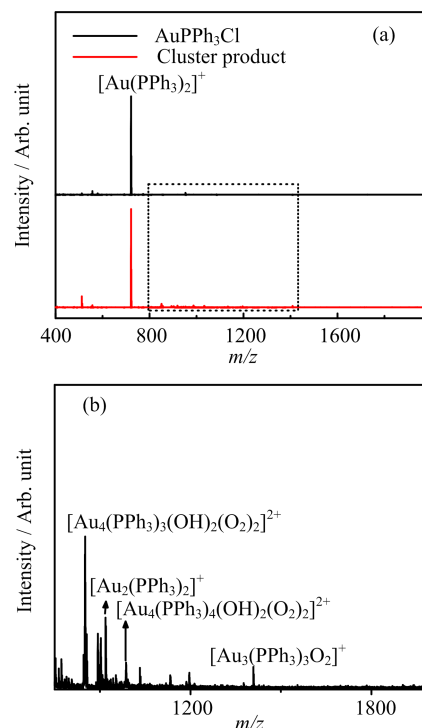
FIG. 1 (a) ESI-MS of the $AuPPh_3Cl$ and the Au_x cluster product over the range of m/z=400−2000, (b) ESI-MS of the Au_x cluster product over the range of m/z=750−2000.

D. Electrocatalytic ORR

A glassy carbon (GC) disk electrode was previously polished with alumina slurries (0.05 μm) and subsequently cleaned by successive sonication in 0.1 mol/L HNO_3, H_2SO_4, and nanopure water for 10 min. The obtained Au_x clusters were dissolved in ethanol (1.0 mg/mL, 10 μL) with the Nafion (10 μL/mL) being added and deposited onto the GC electrode surface (the resulting electrodes were denoted as Au_x/GC) by a Hamilton microliter syringe, which was dried by a gentle nitrogen stream for 2 min. All electrochemical measurements were conducted in a single-compartment glass cell using a standard three-electrode configuration. The reference and counter electrodes were a Ag/AgCl (in 3 mol/L KCl(aq), Bioanalytical systems, MF-2052) and a Pt coil, respectively, with the electrode potentials referred to the Ag/AgCl reference electrode. Both cyclic and linear-sweep voltammetry for oxygen reduction were performed by using a bioanalytical systems (BAS) electrochemical analyzer (Model 100B). And the electrochemical measurements were examined by first bubbling ultrahigh purity oxygen (or purity nitrogen) through the electrolyte solution for at least 15 min and then blanketing the solution with an oxygen atmosphere (or purity nitrogen) during the entire experimental procedure at room temperature.

III. RESULTS AND DISCUSSION

A. Characterization of the ultrasmall gold clusters

The Au$_x$ clusters are prepared according to our facile protocol, as is depicted in detail in the experimental section. For the determination of their molecular formulas, ESI-MS was employed as an essential characteristic tool. The mass spectra of AuPPh$_3$Cl and the cluster product both show intense mass spectrum peak of [Au(PPh$_3$)$_2$]$^+$ at m/z=721 [19], due to its great conductivity in ethanol which restrains the observation of mass spectrum peaks of other species (FIG. 1(a)). In contrast to the featureless signal of AuPPh$_3$Cl mass spectrum over the range of m/z=750$-$1500, many mass spectrum peaks emerge in the mass spectrum of the cluster product, as shown in FIG. 1(b). The mass spectrum exhibits dominant peaks at m/z≈855, 918, 986, and 1409, which are assigned as [Au$_4$(PPh$_3$)$_3$(OH)$_2$(O$_2$)$_2$]$^{2+}$ (theoretical mass: 854.37), [Au$_2$(PPh$_3$)$_2$]$^+$ (theoretical mass: 918.51), [Au$_4$(PPh$_3$)$_4$(OH)$_2$(O$_2$)$_2$]$^{2+}$ (theoretical mass: 985.52), and [Au$_3$(PPh$_3$)$_3$O$_2$]$^+$ (theoretical mass: 1409.77), respectively. The ESI result indicates the Au$_x$ clusters are composed of small gold clusters (x=2,4), whose ligand composition of hydroxyl, and adsorbed oxygen is the same as that of the reported small gold clusters synthesized by exposing the HAuCl$_4$ and sodium citation to the alkaline solution [20].

The chemical nature of the Au$_x$ clusters was studied by XAFS and XPS. Seen from the Au L$_3$-edge X-ray absorption near-edge structure (XANES) spectra (FIG. 2(a)), the Au$_x$ clusters exhibit stronger white-line peak (at ∼11925 eV) than AuPPh$_3$Cl, illustrating more Au 5d electron depleted in Au$_x$, as the white-line arises from the electronic transition from 2p$_{3/2}$ to 5d$_{5/2,3/2}$ of Au atoms. The Fourier transfer of the extended XAFS (EXAFS) spectrum of the Au$_x$ clusters shows a first Au-ligand coordination peak at ∼1.69 Å, which is at a considerably lower position than the Au-P/Cl peak (1.83 Å) of AuPPh$_3$Cl. Considering the Au-O/C peak at ∼1.63 Å reported by Avelino Corma and the co-workers [20] (FIG. 2(b)), the XAFS result further confirmed that the Au$_x$ clusters possess the mixed Au-P/Cl and Au-O coordination. The higher electronegativity of oxygen than sulphur/chlorine atoms leads to the depletion of more Au 5d electrons in the Au$_x$ clusters, in agreement with the XANES observations.

FIG. 3 compares the XPS spectra of the Au$_x$ clusters and AuPPh$_3$Cl. In contrast to the AuPPh$_3$Cl signal, the much higher O 1s peak intensity (FIG. 3(a)) in the XPS survey of the Au$_x$ clusters implied that they are of the main oxygen component. Moreover, the O 1s spectrum of the Au$_x$ clusters displays a strong peak at ∼531.3 eV accompanied by a shoulder at ∼530.8 eV. In agreement with the ESI results, these characteristics could be identified as hydroxyl and absorbed oxygen, which have been reported by Sutthiumporn and the co-workers [21]. The ∼0.2 eV shift to higher Au 4f
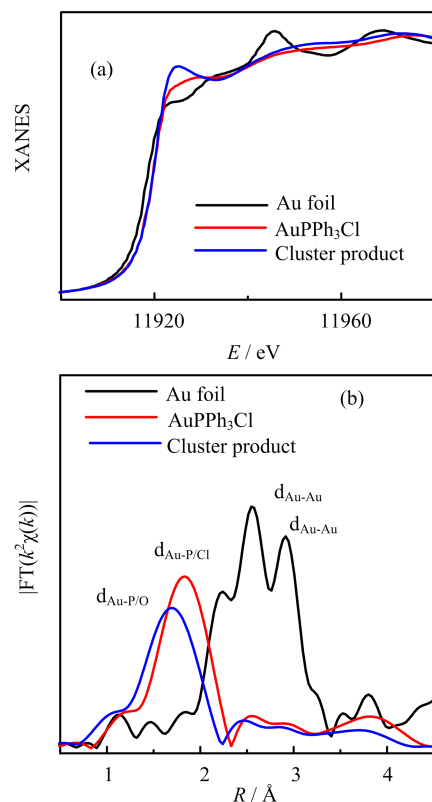

FIG. 2 (a) XANES, and (b) EXAFS spectra of the Au foil, AuPPh$_3$Cl precursor and the cluster product.

binding energy of Au$_x$ again reveals the Au electron depletion (FIG. 3(b)). Summarizing the ESI, XAFS, XPS results, ultrasmall gold clusters with the triphenylphosphine, hydroxyl and adsorbed oxygen ligands have been obtained.

B. Oxygen reduction electrocatalytic activities of the Au$_x$ clusters

The Au$_x$ clusters were loaded onto a glassy carbon electrode (Au$_x$/GC), utilized as electrocatalytic electrode for ORR in 0.1 mol/L KOH aqueous solution. The electrocatalytic activity of the Au$_x$/GC was measured by cyclic and linear-sweep voltammetry. The current density is normalized by the effective Au active surface areas, which is available based on the oxygen adsorption measurement method [22]. The cyclic voltammogram of the Au$_x$/GC electrodes *vs.* RHE shows well-defined cathodic peaks over the potential range from $-$0.33 V to 1.57 V in O$_2$-saturated solution, while no signal is observed in N$_2$-saturated surrounding. It demonstrates that the Au$_x$ clusters are effective electrocatalysts for ORR. The electrocatalytic activity is quantitatively assessed with the two parameters of onset potential and peak current density. FIG. 4(a) shows the current peak density of ∼2.0 mA/cm^2 at the scan rate of 0.1 V/s and
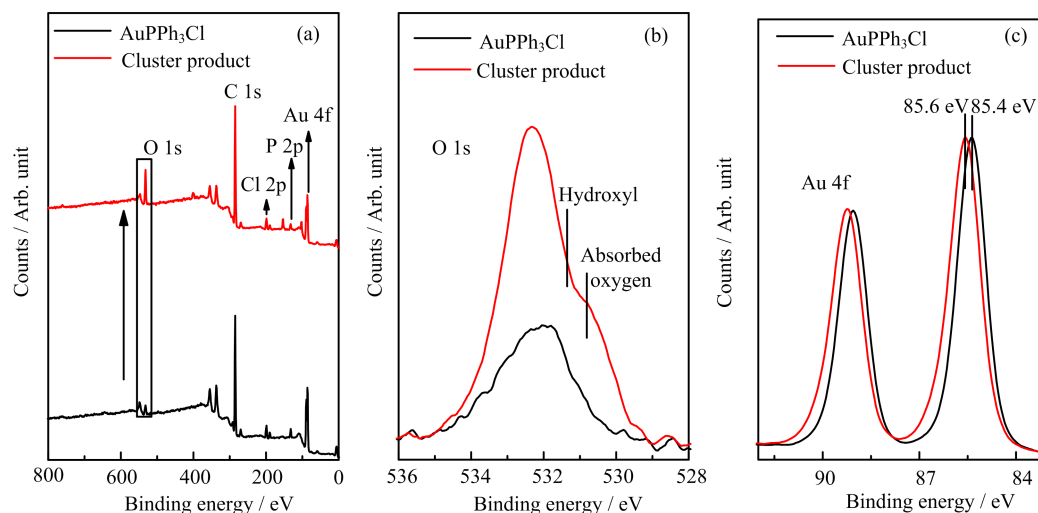
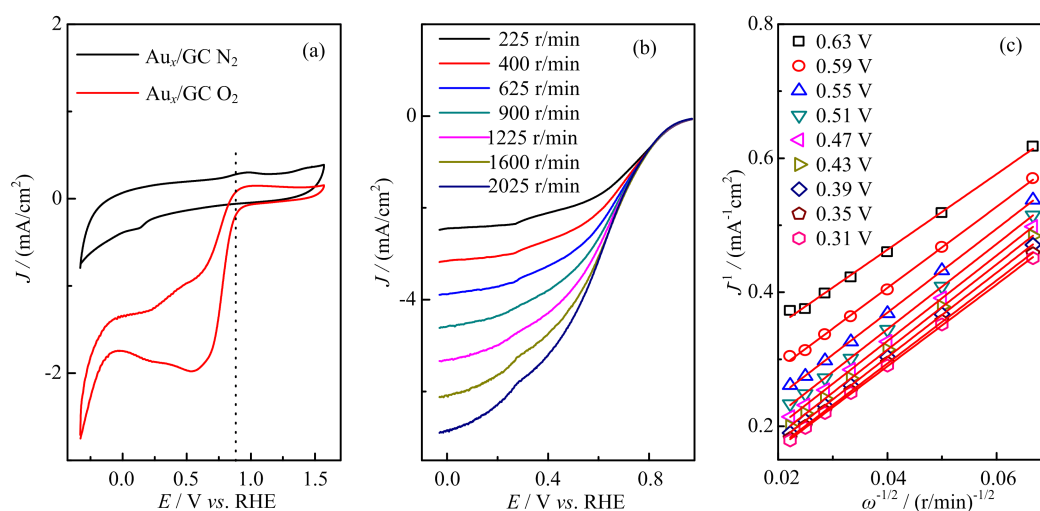FIG. 3 (a) XPS survey, (b) high-resolution O 1s, (c) Au 4f spectra of the AuPPh$_3$Cl and the cluster product.

FIG. 4 (a) Cyclic voltammograms *vs.* RHE of the Au$_x$/GC electrode in the N$_2$- and O$_2$-saturated 0.1 mol/L KOH aqueous solution at the potential scan rate of 0.1 V/s, (b) Linear-sweep voltammograms *vs.* RHE of the Au$_x$/GC electrode at different rotation rates from 225 r/min to 2025 r/min in O$_2$-saturated 0.1 mol/L KOH aqueous solution; and DC ramp 20 mV/s, (c) Koutecky-Levich plots at different potentials from 0.31 V to 0.63 V. Current density is normalized to the effective Au active surface areas. Symbols (FIG. 4(c)) are obtained from the experimental data of the according linear-sweep voltammograms (FIG. 4(b)), and lines are the linear regressions.

the onset potential *vs.* RHE of ~0.87 V.

To further evaluate the kinetic parameters, the Au$_x$/GC was subject to linear-sweep voltammetry measurement at different rotating rates ranging from 225 r/min to 2025 r/min, as shown in FIG. 4(b). The current density increases as the rotating rate increases, which is analogous to those of Au$_{11}$/GC and Pt/GC electrodes reported earlier [18, 23]. The onset potential *vs.* RHE is ~0.87 V, consistent with the cyclic voltammogram result. Furthermore, the corresponding Koutecky-Levich plots (J^{-1} *vs.* $\omega^{-1/2}$) show good linearity and approximately constant slopes at various electrode potentials from 0.31 V to 0.63 V (FIG. 4(c)).

The kinetic parameters can be obtained through the analysis of Koutecky-Levich equations:

$$\frac{1}{J} = \frac{1}{J_K} + \frac{1}{J_L} = \frac{1}{J_K} + \frac{1}{B\omega^{1/2}} \quad (1)$$

$$B = 0.62nFC_O D_O^{2/3}\nu^{-1/6} \quad (2)$$

$$J_K = nFkC_O \quad (3)$$

where J is the measured (total) current density, J_K and J_L are the kinetic and diffusion limiting current densities, respectively, ω is the electrode rotating rate, n is the overall number of electrons transferred, F is the Faraday constant, C_O (1.2×10^{-3} mol/L) is the bulk

concentration of O_2 dissolved in the electrolyte [24], D_O (1.9×10^{-5} cm^{2}s^{-1}) is the diffusion coefficient of O_2 [24], ν (0.01 cm^2/s) is the kinematic viscosity [25], and k is the electron transfer rate constant. From Eq.(1) and Eq.(2), the kinetic current density (J_K) and the number of electrons transferred (n) can be evaluated accordingly from the intercept and the slope of Koutecky-Levich plots, and the electron transfer rate constant (k) can be subsequently obtained according to Eq.(3). Based on these equations, the kinetic parameters of J_K at 0.47 V *vs.* RHE and the number of electrons transferred per O_2 molecule are determined to be 14.28 mA/cm^2 and 3.96, respectively. Based on the obtained parameters of potential onset and current density, the ORR performance of Au$_2$-Au$_4$ is much better than those of Au$_{25}$, Au$_{55}$, Au$_{140}$ and slightly worse than that of Au$_{11}$. The observed behavior is comparable to that of commercial Pt catalysts loaded on carbon, which implies the effective cathode catalyst of the ultrasmall gold clusters for the practical application in fuel-cell electrochemistry.

IV. CONCLUSION

Ultrasmall gold clusters were prepared by a facile method and employed as electrocatalyst for ORR in alkaline solution. The Au$_x$ clusters are identified as small gold clusters of 2−4 Au atoms and triphenylphosphine, oxygen, and hydroxyl ligand. The catalytic behavior of the Au$_x$ clusters for ORR was monitored by cyclic and linear-sweep voltammetry. The obvious reduction current and cathodic peak observed in the cyclic voltammogram reveal the electrocatalytic effectiveness of Au$_x$ clusters with the onset potential *vs.* RHE of ∼0.87 V and current peak density ∼2 mA/cm^2 at the potential scan rate of 0.1 V/s. The kinetic parameters of J_K at 0.47 V and electron-transfer number per O_2 molecule were calculated to be 14.28 mA/cm^2 and 3.96, respectively. This catalytic parameter of onset potential is comparable to that of commercial Pt catalysts loaded on carbon [26], which implies the potential application of ultrasmall gold clusters as electrocatalysts in fuel-cell electrochemistry.

V. ACKNOWLEDGMENTS

[1] Y. H. Bing, H. S. Liu, L. Zhang, D. Ghosh, and J. J. Zhang, Chem. Soc. Rev. **39**, 2184 (2010).

[2] J. Greeley, I. E. L. Stephens, A. S. Bondarenko, T. P. Johansson, H. A. Hansen, T. F. Jaramillo, J. Rossmeisl, I. Chorkendorff, and J. K. Nørskov, Nat. Chem. **1**, 552 (2009).

[3] B. Lim, M. J. Jiang, P. H. C. Camargo, E. C. Cho, J. Tao, X. M. Lu, Y. M. Zhu, and Y. N. Xia, Science **324**, 1302 (2009).

[4] N. M. Marković, H. A. Gasteiger, B. N. Grgur, and P. N. Ross, J. Electroanal. Chem. **467**, 157 (1999).

[5] N. M. Marković, T. J. Schmidt, V. Stamenković, and P. N. Ross, Fuel Cells **1**, 105 (2001).

[6] U. A. Paulus, T. J. Schmidt, H. A. Gasteiger, and R. J. Behm, J. Electroanal. Chem. **495**, 134 (2001).

[7] U. A. Paulus, A. Wokaun, G. G. Scherer, T. J. Schmidt, V. Stamenkovic, V. Radmilovic, N. M. Markovic, and P. N. Ross, J. Phys. Chem. B **106**, 4181 (2002).

[8] Z. M. Peng and H. Yang, J. Am. Chem. Soc. **131**, 7542 (2009).

[9] T. J. Schmidt, U. A. Paulus, H. A. Gasteiger, and R. J. Behm, J. Electroanal. Chem. **508**, 41 (2001).

[10] V. R. Stamenkovic, B. Fowler, B. S. Mun, G. F. Wang, P. N. Ross, C. A. Lucas, and N. M. Marković, Science **315**, 493 (2007).

[11] C. Wang, H. Daimon, and S. H. Sun, Nano Lett. **9**, 1493 (2009).

[12] J. Zhang, K. Sasaki, E. Sutter, and R. R. Adzic, Science **315**, 220 (2007).

[13] J. L. Zhang, M. B. Vukmirovic, K. Sasaki, A. U. Nilekar, M. Mavrikakis, and R. R. Adzic, J. Am. Chem. Soc. **127**, 12480 (2005).

[14] W. Tang, H. F. Lin, A. Kleiman-Shwarsctein, G. D. Stucky, and E. W. McFarland, J. Phys. Chem. C **112**, 10515 (2008).

[15] Y. Z. Lu and W. Chen, J. Power Sources **197**, 107 (2012).

[16] W. T. Wei and W. Chen, Int. J. Smart Nano Mater. **4**, 62 (2013).

[17] J. A. van Bokhoven and J. T. Miller, J. Phys. Chem. C **111**, 9245 (2007).

[18] W. Chen and S. W. Chen, Angew. Chem. Int. Ed. **48**, 4386 (2009).

[19] C. Kowala and J. M. Swan, Aust. J. Chem. **19**, 999 (1966).

[20] A. Corma, P. Concepción, M. Boronat, M. J. Sabater, J. Navas, M. J. Yacaman, E. Larios, A. Posadas, M. A. López-Quintela, D. Buceta, E. Mendoza, G. Guilera, and A. Mayoral, Nat. Chem. **5**, 775 (2013).

[21] K. Sutthiumporn and S. Kawi, Int. J. Hydrogen Energy **36**, 14435 (2011).

[22] S. Trasatti and O. A. Petrii, Pure Appl. Chem. **63**, 711 (1991).

[23] W. Chen, J. Kim, S. H. Sun, and S. W. Chen, J. Phys. Chem. C **112**, 3891 (2008).

[24] R. E. Davis, G. L. Horvath, and C. W. Tobias, Electrochim. Acta **12**, 287 (1967).

[25] A. Sarapuu, M. Nurmik, H. Mändar, A. Rosental, T. Laaksonen, K. Kontturi, D. J. Schiffrin, and K. Tammeveski, J. Electroanal. Chem. **612**, 78 (2008).

[26] K. P. Gong, F. Du, Z. H. Xia, M. Durstock, and L. M. Dai, Science **323**, 760 (2009).